AIAA

AIAA 99-4532
Passive Remote Sensing of Artificial Relativistic Electron Beams in the Middle Atmosphere

L. Habash Krause
Boston College
AFRL/VSBS
Hanscom AFB, MA

T. Neubert
Danish Meteorological Institute
Copenhagen, Denmark

B. E. Gilchrist
University of Michigan
Ann Arbor, MI

Space Technology Conference and Exposition
28-30 September 1999
Albuquerque, NM

Passive Remote Sensing of Artificial Relativistic Electron Beams in the Middle Atmosphere

L. Habash Krause, T. Neubert, and B. E. Gilchrist

Abstract

Two methods of passive remote sensing of mildly (E 5 MeV) relativistic electron beams as they propagate through the Earth's upper and middle atmosphere are presented. Utilization of bremsstrahlung emissions as a diagnostic indicator of beam characteristic energy and particle flux is compared and contrasted with that of the optical emission technique. A new MeV auroral electron model has been developed to compute line emission rates of $O(^1D) \rightarrow O(^3P)$ ($\lambda = 630.0\text{-}636.4$ nm doublet), $O(^1S) \rightarrow O(^1D)$ ($\lambda = 557.7$ nm), $N_2^+(B^3\Sigma_u^+) \rightarrow N_2^+(X^2\Sigma_g^+)$ ($\lambda = 391.4$ nm and 427.8 nm from the N_2^+(1N) band), and $N_2(C^3\Pi_u) \rightarrow N_2(B^3\Pi_g)$ ($\lambda = 337.1$ nm from the N_2(2P) band). The 427.8 nm, 391.4 nm, and 337.1 nm lines are strong in intensity, with production rates several orders of magnitude greater in than those of the O lines examined here. It is shown that the production of 337.1 nm is insensitive to compositional change and has a quenching height lower in altitude than the propagation depth of a 5 MeV electron beam, and thus the signature may be suitable as an indicator of electron flux for beams of comparable energy. The ratio of 427.8 nm to 391.4 nm emissions was found to be relatively insensitive to compositional changes, and the ratio varies with altitude at lower altitudes, suggesting that it may suitable for inference of characteristic beam energy for MeV electron beams. Advantages and disadvantages associated with both the bremsstrahlung and the optical techniques are presented.

Nomenclature

A_d = absolute area of planar detector, cm^2
E = primary electron energy, eV
ℓ_i = loss rate, ith state, /cm^3/s
f = density scaling relative to MSIS-E-90, unitless
n_k = atmospheric neutral number density, kth species, /cm^3
$\wp_i$ = production rate, ith state, /cm^3/s
p_e^k = elastic backscatter coefficient, kth species, /s
q = electron impact ionization rate, /cm^3/s/eV
q^+ = electron cascade /cm^3/s/eV
x_d = detector-source horizontal displacement, km
W = secondary electron energy, eV
z_{bot} = altitude corresponding to beam penetration depth, km
z_{inj} = altitude, beam injection, km
z_{sat} = altitude, LEO diagnostic satellite, km
ϕ = hemispherical electron flux, /cm^2/s/eV
λ = emission wavelength, nm
$\langle\mu\rangle$ = electron flux average pitch angle, rad
σ_a^k = inelastic absorption cross section, kth species, cm^2
σ_e^k = elastic scattering cross section, kth species, cm^2
σ_λ = excitation production cross section, cm^2
θ_d = detector view angle from the vertical, rad
$\Delta\Omega$ = solid angle subtended by effective detector area, sterad
ξ = cross section empirical parameter, unitless

L. Habash Krause is with Boston College, Institute for Scientific Research, and is supported by the Air Force Research Laboratory, Battlespace Environment Division (VSB), 29 Randolph Rd., Hanscom Air Force Base, MA, 01731. E-mail: krause@plh.af.mil.

T. Neubert is with the Danish Meteorological Institute, Solar-Terrestrial Physics Division, Lyngbyvej 100, 2100 Copenhagen 0, Denmark. E-mail: neubert@dmi.min.dk.

B. E. Gilchrist is with the University of Michigan, Space Physics Research Laboratory, 2455 Hayward, Ann Arbor, MI, 48109. E-mail: gilchrst@eecs.umich.edu.

Introduction and Background

With the technology on the horizon to potentially launch a relativistic ($E \sim 5$ MeV) electron beam from an orbiting spacecraft or suborbital sounding rocket [1] comes the challenge of determining the appropriate diagnostic method by which investigators may characterize the propagation of such a beam during an active experiment in space. There are several candidate methods under consideration, including *in situ* beam electron flux measurements, active remote sensing of beam-induced ionization of the atmosphere (*e.g.*, with incoherent scatter radar), and passive remote sensing of radiative emissions associated with

1

the particle precipitation in the atmosphere. We examine here the feasibility of using the passive remote sensing technique as a viable diagnostic for Relativistic Electron Beam (REB) propagation in the Earth's middle atmosphere.

Spaceborne electron beams provide a two-fold utility to space science experimentalists: they may be used to simulate physical processes involving energetic electrons in space and the upper atmosphere/ionosphere, and they may be used to probe distant regions of the near-Earth space environment that are generally inaccessible to *in situ* measurements. For almost three decades, electron beams injected from sounding rockets and Low Earth Orbit (LEO) spacecraft have been helpful in the investigations of numerous topics, including sounding of magnetic field-aligned potential drops in auroral regions [2], magnetic field line tracing within the Earth's inner magnetosphere [3], and generation of artificial aurora [4]. These experiments have incorporated beam accelerators with energies and currents that vary over a broad range. To date, the 40 keV electron beam launched during the ECHO 7 flight [5] represents the electron beam of the highest energy successfully flown, and the 18 A, 2 keV electron beam from the EXCEDE III flight [6] represents the experiment with the highest propagating beam current. The successful injection and propagation of a 5 MeV electron beam would establish the heritage of a spaceborne electron beam that is fully two orders of magnitude greater in energy than any demonstrated flown hardware at the time of this study.

It is postulated that a 5 MeV electron beam could be used to instigate certain space physical processes under controlled conditions. For example, direct simulation of Highly Relativistic Electron events (HREs) would be possible by injection parallel to the Earth's magnetic field and downward into the atmosphere. Controlled experiments of this type would lend tremendous insight into the role of HREs in modification of atmospheric electrodynamics [7] and chemical composition [8]. Other, more esoteric processes such as the triggering of upper atmospheric electrical discharges may be possible if the conductivity modification between a charged thundercloud and the ionosphere is sufficiently large [9]. Alternatively, there is the possibility that seed electrons in the 10's or 100's of keV energy range could be generated in regions of strong electric fields following cloud-to-ground discharges. These electrons may be accelerated to runaway avalanche condition resulting in an upper atmospheric electrical discharge [10].

To assess the feasibility of using MeV electron beams for the applications described above, it is important to establish a viable method by which we can determine the propagating beam character-

istics under a variety of conditions. Beam parameters of interest include total electron energy flux and beam characteristic energy. To this end, this study presents two alternative passive remote sensing methods, bremsstrahlung and optical imaging, which may be used as a diagnostic for a 5 MeV electron beam injected into the Earth's middle atmosphere.

BREMSSTRAHLUNG EMISSIONS

Of the many radiative emissions associated with the slowing down of a mildly relativistic ($E \sim$ MeV) electron beam by the neutral atmosphere, transitional and bremsstrahlung radiation are the most prominent [11]. Even though the bremsstrahlung conversion efficiency during inelastic collisions with the neutral atmosphere is only a few percent for a 5 MeV electron beam propagating in air [11], in spite of this low percentage, bremsstrahlung continues to provide a reliable diagnostic for precipitating energetic electrons due to the penetrating ability of the x-rays [12].

A detailed treatment of the model that simulates bremsstrahlung production and detection can be found in [11], [13], but a brief, qualitative review of the physics is included here. Consider the injection of a 5 MeV electron beam from a sounding rocket at an altitude of 240 km. Injection is toward the Earth and parallel to the Earth's magnetic field, approximated by that of a constant strength of 0.4 G and a dip angle of 90°. The model atmosphere is taken from MSIS-E-90, chosen for its applicability over a wide range of altitudes. As the beam interacts with the atmosphere, the electrons slow down and emit radiation known as bremsstrahlung (literally "braking radiation" in German). The model computes emissions generated from the beam column that propagate through the atmosphere to a planar detector of arbitrary position and orientation in space.

The cross sections illustrated in Figure 1 demonstrate that the probability of photon production decreases with increasing photon energy. However, propagation through the atmosphere results in significant attenuation of photons, especially below 50 keV [14]. Essentially, both the bremsstrahlung production and the photo-absorption cross section decrease with increasing photon energy, so there is a local peak in the x-ray radiation measured at the detector. Processes relevant to high energy photon transport in air, including Compton scattering, the photoelectric effect, Rayleigh scattering, electron-positron pair production, and photonuclear interaction, were considered when computing atmospheric attenuation.

It is noted here that there is a significant amount of high-energy secondary electrons ($W > 50$ keV) resulting from the ionization of the background gas by the primary beam. These fast secondaries
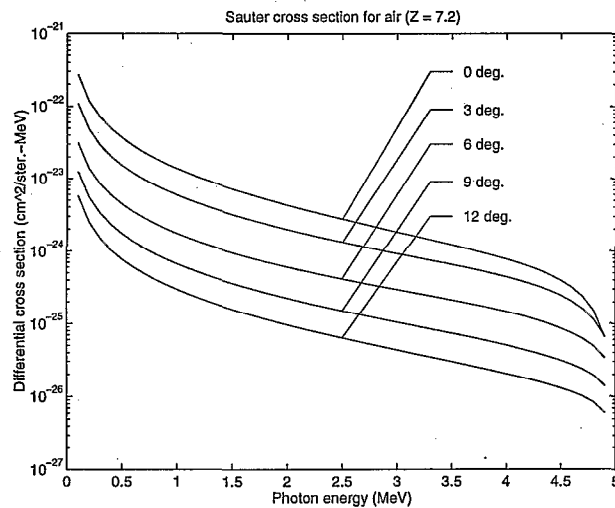
Fig. 1. Sauter cross section, differential in photon energy and emission angle, for a 5 MeV electron beam braking in air.
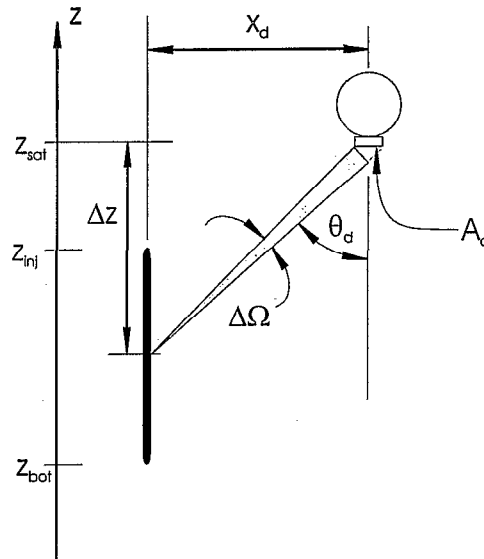
Fig. 2. Schematic of bremsstrahlung flux detection geometry, detection from LEO.

Fig. 3. Integrated bremsstrahlung flux per unit beam electron flux, LEO altitude.

are capable of producing a significant amount of bremsstrahlung emissions, but the vast majority of the photons are of energies less than the 50 keV local peak and are generated at low altitudes [11]. Thus, they are mostly lost to Compton scattering and other processes, so they do not contribute significantly to bremsstrahlung spectra incident on detectors in the configurations examined here. Therefore, we limit our analysis to detection of bremsstrahlung generated by the primary beam only.

First, we examine the case where the detector is aboard a satellite in Low Earth Orbit (LEO). The geometry of the system is given in Figure 2. The bremsstrahlung production column extends from the beam injection altitude (z_{inj}) down to the altitude of maximum penetration depth attainable by the beam (z_{bot}).

Bremsstrahlung production is computed as a function of altitude and emission angle using the differential form of the Sauter-Elwert cross section and the results from the paraxial ray analysis of a 5 MeV beam propagating in a model atmosphere [11]. The beam is injected downwards from an altitude of 240 km, and the satellite altitude is 300 km. Then, the flux incident on the detector is integrated over the entire propagation length of the beam for four cases of horizontal displacement of the satellite from the beam source: $x_d \in [1, 10, 30, \text{ and } 60]$ km. Since it is expected that the photons of energy less than 1 keV will be severely attenuated by the atmosphere, they were not considered in these computations. The resulting fluxes, normalized to the beam electron flux, differential in photon energy, appear in Figure 3. It is evident from this figure that larger amounts of flux

are observed when the detector has a greater horizontal displacement from the radiation source. This is due to the preferential emission of bremsstrahlung in the forward direction. When the detector approaches the horizontal position almost directly overhead the beam source ($x_d = 1$ km), the bremsstrahlung intensity is at a local minimum. As the detector moves farther away from the overhead position, the intensity increases by almost two orders of magnitude when the detector is 60 km away.

Similar computations are completed for the second case in which the detector is now on a balloon at an altitude of 39 km, and the detector is oriented so that it is perpendicular to the Earth's surface and faces the base of the propagating beam. As in the
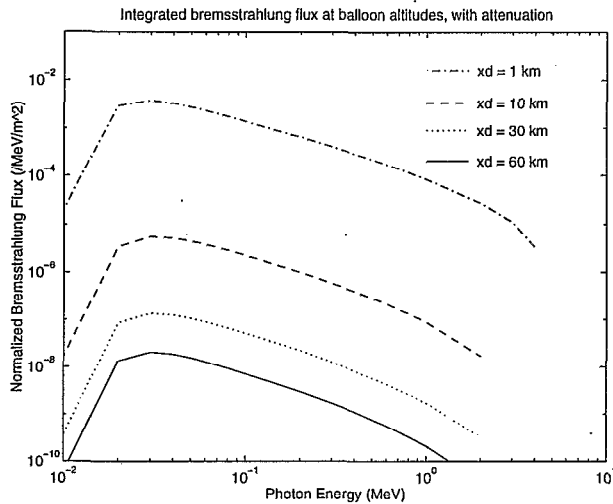
3

Fig. 4. Integrated bremsstrahlung flux per unit beam electron flux, balloon altitude.

LEO case, integrated bremsstrahlung was computed for four horizontal detector displacements. Since the detector is now at the base of the propagation, reducing the horizontal displacement results in increased measured bremsstrahlung flux compared with larger displacements (Figure 4). Note that for the cases examined here, the measured bremsstrahlung flux is significantly greater at the balloon detectors than it is at the satellite detectors.

OPTICAL EMISSIONS

The technique of interpreting optical auroral data to determine the characteristic energy and total energy flux of precipitating electrons is well established. For example, since the 427.8 nm from the N_2^+(1N)(0,1) band is an allowed transition, there is a one-to-one correspondence between total precipitating electron energy flux and the photon flux integrated along the line of sight between the emission column and the imager. Ratios of line intensities can be useful for determination of characteristic electron energy if one of the emissions is from a metastable state. For example, consider the 630.0-636.4 nm doublet which originates from the $O(^1D)$ state. $O(^1D)$ is a metastable state with a lifetime of 110 s. Quenching is a major loss process for $O(^1D)$, becoming particularly significant as the precipitating electrons reach lower altitudes where quenching constituents become increasingly abundant. So, there is a one-to-one correspondence between the depth of penetration of the electron beam with the ratio of 630-36 nm emission to 427.8 nm: the larger the ratio, the higher in altitude the beam was stopped (signifying lower beam energy). Note however that the accuracy of this technique depends on the that of the neutral atmospheric density model [15].

Until now, this technique has been successfully demonstrated for electrons up to 10's of keV in energy. We propose that the method would be equally suitable for MeV electron beams. The justification is thus: the bulk of the energy lost due to inelastic collisions in air goes to ionization of the background gas. These secondaries are extremely energetic, with e-folding energies of approximately 50 keV. Therefore, they can be considered as incremental sources of aurora along the track of the ionization trail created by the beam.

The transitional radiation emission model begins with the computations of energetic secondaries from the initial beam-atmosphere interaction and the resulting production rates of excited atomic and molecular states. Electron cascading in energy is modeled by the solution of the coupled two stream equations, expressed here in the local approximation:

$$\phi^+ = \frac{1}{\sum_k n_k[\sigma_a^k + p_e^k \sigma_e^k]} \left[\sum_k n_k p_e^k \sigma_e^k \phi^- + \frac{q}{2}\langle \mu \rangle + q^+ \right] \tag{1}$$

$$\phi^- = \frac{1}{\sum_k n_k[\sigma_a^k + p_e^k \sigma_e^k]} \left[\sum_k n_k p_e^k \sigma_e^k \phi^+ + \frac{q}{2}\langle \mu \rangle + q^+ \right] \tag{2}$$

where $\phi^{+(-)}$ represents the zenith (nadir) directed hemispherical electron fluxes differential in energy and as a function of altitude. The bracketed terms from left to right represent the contribution to the hemispherical flux due to elastic backscatter from the opposing hemisphere, production by electron-impact ionization of ambient neutral constituents, and cascading from higher energies. The denominator represents reduction in flux due to inelastic absorption and elastic basckscatter into the opposing hemisphere.

These electron fluxes are incorporated into a chemistry model to compute time dependent emission rates resulting from the steady pumping of fast electrons into the atmosphere. The lines of interest and their corresponding transitions appear in Table I. These forbidden transitions of O and allowed transitions of N_2^+(1N) (427.8 nm and 391.4 nm) and N_2(2P) (337.1 nm) were selected for comparison with established auroral observational techniques. Chemical reactions contributing to the production and loss of the excited state densities are listed with the appropriate rate coefficients in Table II.

The chemistry model requires the solution of the set of continuity equations representing the evolution of the densities of chemical species over time. Following *Strickland et al.* [15], we: 1) neglect ion and neutral transport in the E and lower F regions, and 2) begin with a model atmosphere for major neutral

Type	Reaction	Rate Coefficient
EI	$e_f + O_2 \rightarrow O_2^+ + e_f + e$	
EI	$e_f + O \rightarrow O(^1D) + e_f$	
EI	$e_f + O \rightarrow O(^1S) + e_f$	
EI	$e_f + O \rightarrow O^+ + e_f + e$	
EI	$e_f + N_2 \rightarrow N_2^+(B^2\Sigma_u^+) + e_f + e$	
EI	$e_f + N_2 \rightarrow N_2^+(C^3\Pi_u) + e_f$	
DR	$e_{th} + O_2^+ \rightarrow O + O(^1D)$	$k_5 = 2.2(-7) \times (300/T_e)^{1/2}$
DR	$e_{th} + O_2^+ \rightarrow O + O(^1S)$	$k_{5a} = 0.1k_5$
EI	$e_f + N_2 \rightarrow N^+ + N + e_f + e$	
CE	$N_2^+ + O_2 \rightarrow O_2^+ + N_2$	$k_7 = 5.1(-11) \times (T_{th}/300)^{-4/5}$
CE	$O^+ + O_2 \rightarrow O_2^+ + O$	$k_8 = 2.0(-11) \times (T_{th}/300)^{-4/5}$
CE	$N^+ + O_2 \rightarrow O_2^+ + N$	$k_9 = 6.0(-10)$
Q	$O(^1D) + N_2 \rightarrow O + N_2$	$k_{10} = 2.7(-11)$
Q	$O(^1D) + O_2 \rightarrow O + O_2$	$k_{11} = 3.6(-11)$
Q	$O(^1D) + NO \rightarrow O + NO$	$k_{12} = 3.5(-11)$
Q	$N_2^+(B^2\Sigma_u^+) + O_2 \rightarrow N_2^+ + O_2$	$k_{13} = 4.0(-10)$
Q	$O(^1S) + O \rightarrow O + O$	$k_{14} = 7.5(-12)$
Q	$O(^1S) + O_2 \rightarrow O + O_2$	$k_{15} = 3.0(-13)$
EI	$N(^4S) + e_f \rightarrow N(^2D)$	
ET	$N(^2D) + O_2 \rightarrow NO + O(^1D)$	$k_{16a} = 6.0(-13)$
ET	$NO + N(^4S) \rightarrow N_2 + O$	$k_{17} = 2.2(-11)$
CE	$N_2^+ + O \rightarrow N(^2D) + NO^+$	$k_{18} = .25 \times 1.4(-10)$
DR	$NO^+ + e_{th} \rightarrow N(^2D) + O$	$k_{19} = .5 \times 6.1(-7) \times (300/T_e)^{9/5}$
Q	$N(^2D) + O_2 \rightarrow N(^4S) + O_2$	$k_{20} = 6.0(-12)$
Q	$N(^2D) + O \rightarrow N(^4S) + O$	$k_{21} = 5.0(-13)$
Q	$N(^2D) + NO \rightarrow N(^4S) + NO$	$k_{22} = 6.3(-11)$
CE	$NO + O_2^+ \rightarrow NO^+ + O_2$	$k_{23} = 4.4(-10)$
SE	$O(^1D) \rightarrow O + h\nu$	$A_1 = 9.1(-3)$
SE	$O(^1S) \rightarrow O + h\nu$	$A_2 = 1.22$
SE	$N_2^+(B^2\Sigma_u^+) \rightarrow N_2^+ + h\nu$	$A_3 = 1.4(7)$
SE	$N_2(C^3\Pi_u) \rightarrow N_2 + h\nu$	$A_4 = 2.0(7)$
SE	$N(^2D) \rightarrow N(^4S) + h\nu$	$A_5 = 1.1(-5)$

TABLE II

CHEMICAL REACTIONS INCLUDED IN THE MODEL. REACTION TYPES INCLUDE DIRECT FAST ELECTRON IMPACT (EI), DISSOCIATIVE RECOMBINATION (DR), CHARGE EXCHANGE (CE), QUENCHING (Q), ENERGY TRANSFER (ET), AND SPONTANEOUS (TRANSITIONAL) EMISSION (SE). SHORTHAND NOTATION OF REACTION RATE COEFFICIENTS: 2.2(-7) IS EQUIVALENT TO 2.2×10^{-7}. UNITS: k VALUES IN $CM^3 S^{-1}$; A VALUES IN S^{-1}. ELECTRON IMPACT REACTIONS DO NOT REQUIRE RATE COEFFICIENTS.

constituents (O, O_2, and N_2), and apply *ad hoc* scaling factors, ranging from 0.7 to 1.5, to account for compositional changes of O and O_2 densities relative to that of N_2. Then, we have a system of ordinary differential equations that represent the change in species density with time. The continuity equations are of the form:

$$\frac{dn_{O(1D)}}{dt} = \wp_{O(1D)} - \ell_{O(1D)} \qquad (3)$$

Here, $\wp_i = \wp_i(z,t)$ represents the production of the ith excited state due to impact on ambient neutrals by all fast electrons (the dense secondaries from the initial beam-atmosphere interaction) and

the relevant chemistry from Table II; $\ell_i = \ell_i(z,t)$ is the chemical loss term (quenching, charge exchange, *etc.*). The set is completed with the addition of the continuity equations for $O(^1S)$, O^+, O_2^+], N, $N(^2D)$, N^+, N_2^+, $N_2^+(B^2\Sigma_u^+)$, $N_2(C^3\Pi_u)$, NO, and NO^+.

The cross sections for the excited state production are of the semi-empirical form employed by Green and Stolarski:

$$\sigma_\lambda(E) = \frac{q_o \xi_1}{W^2} \left(1 - \left(\frac{W}{E}\right)^{\xi_2} \right)^{\xi_3} \left(\frac{W}{E}\right)^{\xi_4} \qquad (4)$$

where ξ_{1-4} are unitless empirically derived quanti-

5

Transition	λ (nm)
$O(^1D) \rightarrow O(^3P)$	630.0-636.4 (doublet)
$O(^1S) \rightarrow O(^1D)$	557.7
$N_2^+(B^2\Sigma_u^+, v'=0) \rightarrow N_2^+(X^2\Sigma_g^+, v''=1)$	427.8
$N_2^+(B^2\Sigma_u^+, v'=0) \rightarrow N_2^+(X^2\Sigma_g^+, v''=0)$	391.4
$N_2(C^3\Pi_u, v'=0) \rightarrow N_2(B^3\Pi_g, v''=0)$	337.1

TABLE I

OPTICAL EMISSION LINES OF INTEREST.

N_2 State	W (eV)	ξ_1	ξ_2	ξ_3	ξ_4
$C^3\Pi_u$	11.03	0.28	3	1.5	3

O State	W (eV)	ξ_1	ξ_2	ξ_3	ξ_4
^1D	1.96	0.01	1.0	2.0	1.0
^1S	4.18	4.2e-3	0.5	1.0	1.0

TABLE III

SEMI-EMPIRICAL EXCITATION CROSS SECTION PARAMETERS

Fig. 5. Excited state production rates for O(1D) (solid), O(1S) (dash-dot), $N_2(C^3\Pi_u)$ (dash), and $N_2^+(B^3\Sigma_u^+)$ (dot).

Fig. 6. Emission yields for red (solid) and green (dash-dot) lines, 1 μs source, 0.5 second integration time.

ties and are listed in Table III for atomic oxygen and neutral molecular nitrogen. Widely accepted branching ratios are used with molecular nitrogen ionization rates to compute the production of N_2^+ by electron impact ionization of N_2: 76% of N_2 ionization events result in N_2^+ production, and of these events, 11% result in the $N_2^+(B^2\Sigma_u^+)$ state. State densities are multiplied by the appropriate spontaneous transition coefficient, yielding time-dependent line emission rates as a function of altitude.

We now consider the emission of red (630.0-636.4 nm), green (557.7 nm), blue (427.8 nm), UV1 (337.1 nm), and UV2 (391.4 nm) lines integrated over a one second time interval. The electron source is a 5 MeV, 1.0 A, 1.0 μs pulse with a square shape (instantaneous rise and fall time). The viewing integration time is 0.5 seconds. Similar to the computations in the previous section, the beam is injected downward from an altitude of 240 km parallel to the Earth's magnetic field, which is approximated as having a 90° dip angle and a constant strength of 0.4 G. Hemispherical electron fluxes are first computed as a function of altitude. The resulting excited state production densities solely from electron impact of ambient neutrals appear in Figure 5.

Production rates of $O(^1D)$ and $O(^1S)$ excited states peak at 90 km and fall off rapidly as lower altitudes are reached, following the density reduction of ambient O. The molecular nitrogen states follow the energy deposition profile of the beam, increasing rapidly until the beam loses all of its energy at the altitude corresponding to the beam penetration depth,
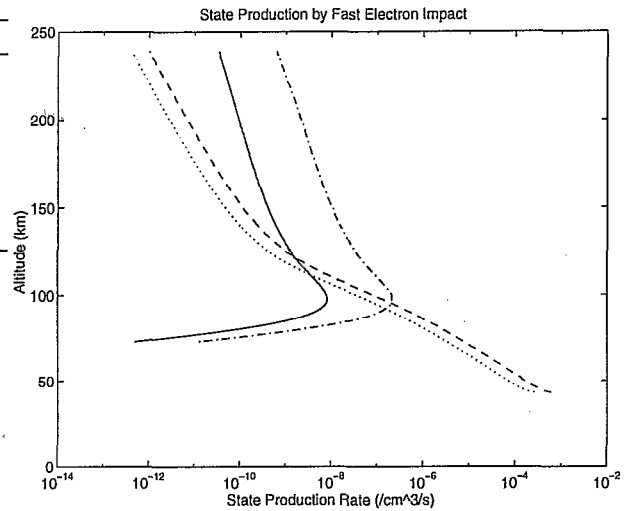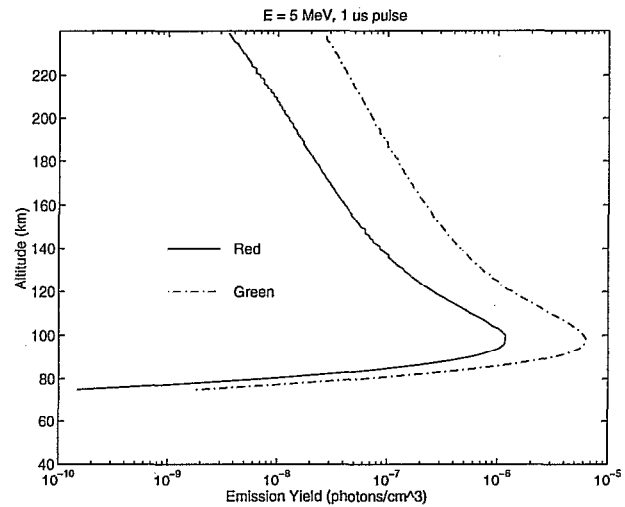
approximately 43 km for the 5 MeV beam.

Red and green line emission rates appear in Figure 6. Both emissions have strong peaks at roughly 95 km in altitude, but they fall off rapidly due to a decrease in ambient O density and an increase in quenching effects. The overall emission rate is weak, signifying that red and green would be poor diagnostic indicators for MeV electron beams. This is not surprising considering that nadir-directed MeV beams lose relatively little energy above 75 km in altitude [13].

Blue, UV1, and UV2 line emissions appear in Figure 7. Here we see that the signatures are strong, reaching values of over 1000 photons/cm^3. Toward the end of the propagation, between the altitudes of 80 and 40 km, the emission yields appear to be constant or even decreasing with propagation depth.
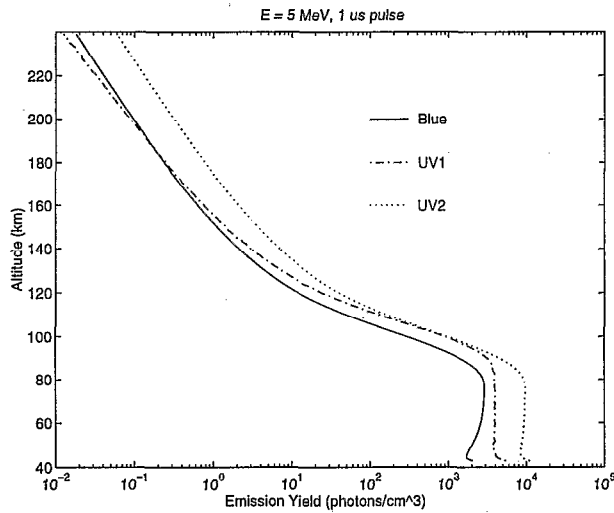
6

Fig. 7. Emission yields for blue, UV1, and UV2 lines, 1 μs source 0.5 second integration time.
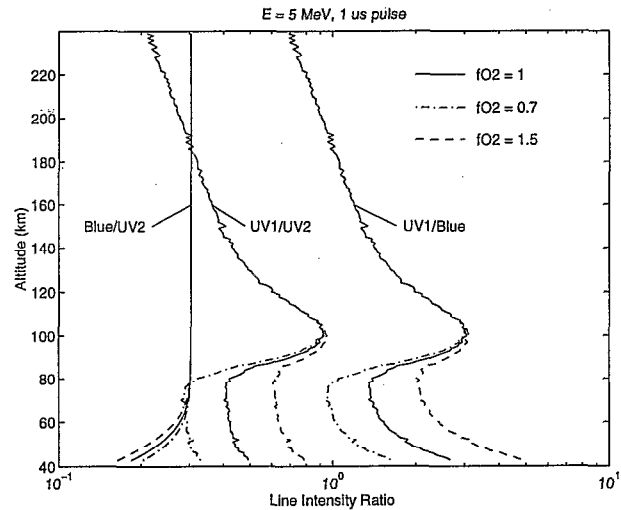

Fig. 9. Ratios of blue, UV1 and UV2 line emission rates and their dependence on fO2, 1 μs source 0.5 second integration time.
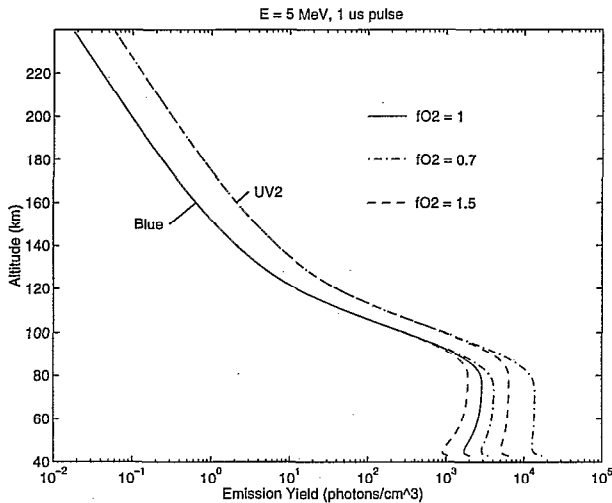

Fig. 8. Blue and UV2 line emission yield dependence on fO2, 1 μs source 0.5 second integration time.

This is because although the beam is converting more total energy to optical emissions as it propagates deeper in the atmosphere, it is radially expanding rapidly in this particular region [11]. This dilutes the density of photon emissions as the total number increases, an effect which manifests itself as an emission rate approximately constant with altitude.

We now examine the effect of compositional scaling on emission yields of the blue, UV1, and UV2 lines. From Figure 8, it is apparent that scaling the O_2 density by fO2 = 0.7 and 1.5 makes a significant impact on the blue and UV2 signatures in the lower altitudes (z below 80 km, roughly); O_2 scaling between 0.7 and 1.5 resulted in a change of UV1 emission rate of less than 1%. The model demonstrated that scaling by fO = 0.7 through 1.5 did not significantly affect any of the blue, UV1, or UV2 emission rates.

Figure 9 illustrates the ratios of blue to UV2, UV1 to UV2, and UV1 to blue as a function of altitude. Also shown is the dependence on atmospheric composition. We first note that UV1/UV2 and UV1/blue exhibit a strong dependence on altitude and composition. Blue/UV2 is independent of altitude until the beam reaches the latter stages of propagation below 70 km; this ratio is also fairly independent of compositional change, similar to the aurora from keV electron precipitation [17]. Recall that blue and UV2 originate from the $N_2^+(B^3\Sigma_u^+)$ state, and UV1 originates from the $N_2(C^3\Pi_u)$ state. Quenching by O is negligible to both of these states, so it is little surprise that the emissions from the $N_2^+(1N)$ and $N_2(2P)$ bands are insensitive to the fO scaling. Quenching by O_2, however, was considered to be significant to both bands, although the quenching height of $N_2^+(1N)$ is higher in altitude than that of $N_2(2P)$: 48 km versus 36 km [18]. For this reason, UV1 is not significantly affected by the O_2 mixing ratio, whereas blue and UV2 do exhibit sensitivity to the composition. For MeV electron aurora, the UV1 line provides a direct one-to-one relationship with particle flux independent of oxygen concentration.

If is shown that blue/UV2 is sensitive to beam characteristic energy, it would be a viable diagnostic for MeV electrons due to its independence of atmospheric composition. It has been demonstrated previously that this ratio is *not* a viable diagnostic for keV electrons, but that may be due to the fact that the auroral production occurs at altitudes where quenching is not a significant source of $N_2^+(1N)$ loss. Noting that an increase in quenching as the beam propagates to lower altitudes is enough to modify blue/UV2 at those altitudes, there is hope that this

7

ratio is sensitive to penetration depth, and therefore, characteristic beam energy.

DISCUSSION

The advantages of using the bremsstrahlung technique are that the method is well-established, the emissions propagate to balloon altitudes, and that a detailed neutral atmospheric model is not necessary for accurate results. The principal disadvantage is the weak intensity of the signature, especially when viewed from behind the propagating beam. That is, preferable viewing geometry should be planned to intercept emissions within the forward hemisphere of the propagating beam. During the experiment, this may or may not be practical. It is not always predictable where the beam will precipitate, especially when one considers interhemispherical propagation. Conversely, viewing in the nadir direction from a satellite does offer the advantage of a wide footprint since increasing horizontal displacement increases the amount observed flux until a maximum.

The optical technique is well-established for precipitating electrons with energies of 10's of keV, and the extension to MeV electrons can be verified experimentally with companion measurements using other techniques, both of passive (*e.g.*, bremsstrahlung) and active (*e.g.*, incoherent scatter radar) in nature. Since the atmosphere is optically transparent to the lines considered in this study, viewing from ground, balloon, and satellite is possible. The principle disadvantage to the optical technique is that an accurate neutral atmospheric model, one which correctly predicts the density of O_2, may be necessary when certain lines are considered (*e.g.*, blue and UV2).

Once a reliable technique of diagnosing REB deposition in the atmosphere is established, we can investigate the efficiency of the conjugate magnetic mirroring effect as a method of reflecting MeV particles. The ability to image the precipitating electron spectra following a bounce off of the conjugate magnetic mirror would be helpful for the investigation of the physics associated with this process, one which is of fundamental importance to those investigating MeV electrons trapped in the Earth's magnetosphere. Also, space-based injection of MeV electron beams has a promising application as a tool of active remote sensing of the neutral atmosphere in areas that are difficult to reach by *in situ* methods. For example, with a beam of known characteristic energy and particle flux, we can inject the beam into a region of the atmosphere, and by recording the intensity of various line emissions of interest, we can determine the density scaling factors of the neutral constituent relative to a model atmosphere. This technique has been utilized passively with naturally occurring aurora [19], so the extension to artificial probes is fea-

sible and yet another exciting application of active space experiments with relativistic electron beams.

REFERENCES

[1] Jost, J., Spaceborne relativistic electron accelerator system, Final Report, SBIR Program, Topic Number AF92-084, 1993.

[2] Kellog, P. J., Electron beams and their interaction with the ionosphere - A review of the E∥B series, *Adv. Space Res.*, *12*, 12(15)-12(28), 1992.

[3] Winkler, J. R., Controlled experiments in the Earth's magnetosphere with artificial electron beams, *Rev. Mod. Phys.*, *64*, 859-871, 1992.

[4] Neubert, T., J. L. Burch, and S. B. Mende, The SEPAC artificial aurora, *Geophys. Res. Lett.*, *22*, 2469-2472, 1995.

[5] Nemzek, R. J., and J. R. Winckler, Electron beam sounding rocket experiments for probing the distant magnetosphere, *Phys. Rev. Lett.*, *67*, 987-990, 1991.

[6] Rappaport, S. A., R. J. Rieder, W. P. Reidy, R. L. McNutt, Jr., and J. J. Atkinson, Remote x-ray measurements of the electron beam from the EXCEDE III experiment, *J. Geophys. Res.*, *98*, 19093-19098, 1993.

[7] Goldberg, R. A., C. L. Croskey, L. C. Hale, J. D. Mitchell, and J. R. Barcus, Electrodynamic response of the middle atmosphere to auroral pulsations, *J. Atmosph. Terr. Phys.*, *34*, 1067-1084, 1990.

[8] Callis, L. B., D. N. Baker, J. B. Blake, J. D. Lambeth, R. E. Boughner, M. Natarajan., R. W. Klebesadel, and D. J. Gourney, Precipitating relativistic electrons: Their long-term effect on stratospheric odd nitrogen levels, *J. Geophys. Res.*, *96*, 2939-2976, 1991.

[9] Neubert, T., B. E. Gilchrist, S. Wilderman, L. Habash, and H. J. Wang, Relativistic Electron Beam Propagation in the Earth's Atmosphere: Modeling Results, *Geophys. Res. Lett.*, *23*, 1009-1012, 1996.

[10] Gurevich, A. V., J. A. Valdivia, G. M. Milikh, and K. Papadopoulos, Runaway electrons in the atmosphere in the presence of a magnetic field, *Radio Sci.*, *31*, 1541-1554, 1996.

[11] Habash Krause, L., *The Interaction of Relativistic Electron Beams with the Near-Earth Space Environment*, University of Michigan, Ph.D. Dissertation, 1998.

[12] Rees, M. H., Ionization in the Earth's atmosphere by aurorally associated bremsstrahlung X-rays, *Planet. Space Sci.*, *12*, 1093-1108, 1964.

[13] Habash Krause, L., B. E. Gilchrist, and T. Neubert, Analysis of Active Space Experiments Using Relativistic Electron Beams, *Proceedings of the 6th Spacecraft Charging and Technology Conference, Hanscom AFB, Nov. 1998*, in press, 1999.

[14] Berger, M. J., and S. M. Seltzer, Bremsstrahlung in the Atmosphere *J. Atmosph. Terr. Phys.*, *34*, 85-108, 1972.

[15] Strickland, D. J., R. R. Meier, J. H. Hecht, and A. B. Christensen, Deducing composition and incident electron spectra from ground-based auroral optical measurements: Theory and model results, *J. Geophys. Res.*, *94*, 13527-13539, 1989.

[16] Green, A. E. S., and R. S. Stolarski, Analytic models of electron impact cross sections, *J. Atmosph. Terr. Phys.*, *34*, 1703-1717, 1972.

[17] Rees, M. H., and D. Lummerzheim, Characteristics of auroral electron precipitation derived from optical spectroscopy, *J. Geophys. Res.*, *94*, 6799-6815, 1989.

[18] Vallance Jones, A., *Aurora*, D. Reidel Publishing Company, Dordrecht, Holland, 1974.

[19] Hecht, J. H., A. B. Christensen, D. J. Strickland, and R. R. Meier, Deducing composition and incident electron spectra from ground-based auroral optical measurements: Variations in Oxygen density, *J. Geophys. Res.*, *94*, 13553-13563, 1989.